ELSEVIER

Composite Structures 52 (2001) 3–11

COMPOSITE STRUCTURES

www.elsevier.com/locate/compstruct

Thermal effects on laminated composite shells containing interfacial imperfections

Zhen-Qiang Cheng [a,*,1], R.C. Batra [b]

[a] *Department of Modern Mechanics, University of Science and Technology of China, Hefei, Anhui 230026, People's Republic of China*
[b] *Department of Engineering Science and Mechanics, Virginia Polytechnic Institute and State University, Blacksburg, VA 24061, USA*

Abstract

The effect of thermal loads on imperfectly bonded laminated composite shells is studied. The interfacial imperfections necessitate that conditions requiring the continuity of surface tractions and displacements between adjoining faces be suitably modified, and interfacial damage properly accounted for. Both mechanical and thermal interfacial imperfections are characterized by interfacial parameters in the non-linear equations of motions. Results are presented for two static linear problems. © 2001 Elsevier Science Ltd. All rights reserved.

Keywords: Laminated shell; Interfacial sliding; Thermomechanical deformation

1. Introduction

Laminated composite structures are widely used in mechanical, aeronautical and aerospace applications. Significant changes in material properties across the material interfaces in laminated structures can enhance the rate of debonding between the adjoining layers. Different cases of reduced adhesion (interfacial contact) in composites, such as cleavages, cracks, non-adhesion, slippage zones and similar imperfections, can arise as a consequence of the manufacturing technology and/or operating conditions. In some circumstances, the initiation of decohesion and gross failure occur simultaneously. In other circumstances, considerable additional deformation happens before complete failure of the part so that the progressive change in the deformation pattern due to decohesion needs to be determined.

Separation along interfaces plays a key role in limiting the ductility and toughness of a wide variety of solids. Key parameters characterizing the elastic interface response are the interface strength and the work of separation per unit area which are presumed to reflect the interface structure and chemistry. A phenomenological framework for describing the process of initial interfacial debonding through complete separation has been described by Needleman [1]. The interface is characterized by a traction-displacement relation and dimensional considerations introduce a characteristic length. For displacement jumps across the interface limited to values much smaller than the characteristic length, a linear interfacial model was proposed by Aboudi [2]. The linear interface model has been used for modeling the mechanical behavior of composite laminated beams, plates and shells with interlaminar imperfections [3–18] and numerical examples have revealed the important influences of imperfect interface debonding.

As mechanical, aeronautical and aerospace structural systems are exposed to severe environmental conditions, hygrothermal effects such as thermal expansion, and swelling and shrinkage due to the changes in the moisture content are common in such structures. Thus the analysis of hygrothermal effects on structural systems is important. Here, we study the effects of thermal loads on composite laminated shells containing interfacial imperfections. The problem formulation accounts for both mechanical and thermal interfacial imperfections characterized by interfacial parameters. In an illustrative problem, the temperature field is solved analytically, and its influence on the laminated composite shells with imperfect interfaces is scrutinized.

* Corresponding author. Tel.: +1-979-862-4037; fax: +1-979-862-3989.
E-mail address: chengz@isc.tamu.edu (Z.-Q. Cheng).
[1] Visiting Research Associate, was at Virginia Polytechnic Institute and State University.

PII: S0263-8223(00)00197-5

2. Governing equations and boundary conditions

We consider a laminated shell, shown in Fig. 1, that in the unstressed reference configuration consists of k homogeneous and anisotropic layers of uniform thicknesses, and use a curvilinear coordinate system $\{\theta^i\}$ $(i=1,2,3)$ to describe its deformations. The θ^3-axis is normal to the shell surface, and the reference surface is chosen to be the bottom surface, $\theta^3=0$, of the shell. The bottom surface $(m=0)$, the $k-1$ interfaces $(m=1,\ldots,k-1)$ and the top surface $(m=k)$ are denoted by ${}^{(m)}\Omega(m=0,\ldots,k)$. Thus, the mth layer in the θ^3-direction extends from ${}^{(m-1)}h$ to ${}^{(m)}h$, where ${}^{(m)}h(m=0,\ldots,k)$ is the distance between ${}^{(m)}\Omega$ and ${}^{(0)}\Omega$. In particular, ${}^{(0)}h=0$, ${}^{(k)}h=h$, where h is the total thickness of the shell.

Hereafter, $()_{,i}$ denotes a partial derivative with respect to θ^i, while $()_{\|i}$ and $()_{|\alpha}$ designate covariant derivatives with respect to the space and the reference surface metrics, respectively. A repeated index implies summation over the range of the index with Latin indices ranging from 1 to 3 and Greek indices from 1 to 2. A dot over a quantity refers to a derivative with respect to time, t.

Let the covariant base vectors $\mathbf{a}_i$ and contravariant base vectors $\mathbf{a}^i$ of the reference surface and the space covariant base vectors $\mathbf{g}_i$ and contravariant base vectors $\mathbf{g}^i$ be introduced in the undeformed state of the shell, with

$$\begin{aligned}&\mathbf{a}^3=\mathbf{a}_3=\frac{\mathbf{a}_1\times\mathbf{a}_2}{|\mathbf{a}_1\times\mathbf{a}_2|},\quad \mathbf{g}_\alpha=\mu_\alpha^\beta\mathbf{a}_\beta,\quad \mathbf{g}_3=\mathbf{a}_3,\\&\mathbf{g}^\beta=(\mu^{-1})_\alpha^\beta\mathbf{a}^\alpha,\quad \mathbf{g}^3=\mathbf{a}^3,\end{aligned}\tag{1}$$

where μ_α^β denotes the shifter tensor generalized for composite laminated shells and is non-singular. μ_α^β, its inverse $(\mu^{-1})_\alpha^\beta$ and its determinant μ are given by

$$\begin{aligned}&\mu_\alpha^\beta=\delta_\alpha^\beta-\theta^3 b_\alpha^\beta,\quad (\mu^{-1})_\alpha^\beta=\frac{1}{\mu}\varepsilon^{\beta\lambda}\varepsilon_{\alpha\nu}\mu_\lambda^\nu,\\&\mu=\det(\mu_\alpha^\beta),\end{aligned}\tag{2}$$

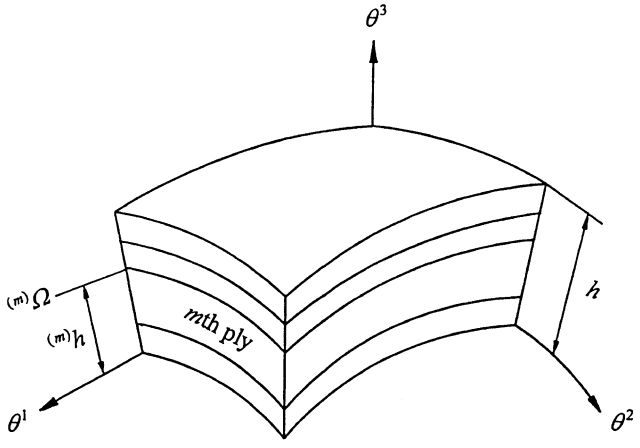

Fig. 1. Geometry of a laminated shell.

where δ_α^β is the Kronecker delta function, $\varepsilon^{\beta\lambda}$ and $\varepsilon_{\alpha\nu}$ are the two-dimensional permutation tensors, and

$$\begin{aligned}&b_\alpha^\beta=b_{\alpha\gamma}a^{\beta\gamma}=-\Gamma_{\alpha3}^\beta\,|_{(0)_\Omega},\\&b_{\alpha\beta}=-\mathbf{a}_\alpha\cdot\mathbf{a}_{3,\beta}=\mathbf{a}_3\cdot\mathbf{a}_{\alpha,\beta}=\Gamma_{\alpha\beta}^3\,|_{(0)_\Omega}.\end{aligned}\tag{3}$$

b_α^β is the mixed curvature tensor, $b_{\alpha\beta}$ is the coefficient of second fundamental form of the reference surface ${}^{(0)}\Omega$, and Γ_{jk}^i denotes the Christoffel symbol of the second kind. The components of the metric tensor for the undeformed reference surface are

$$\begin{aligned}&a_{\alpha\beta}=\mathbf{a}_\alpha\cdot\mathbf{a}_\beta,\quad a_{\alpha3}=\mathbf{a}_\alpha\cdot\mathbf{a}_3=0,\quad a_{33}=\mathbf{a}_3\cdot\mathbf{a}_3=1,\\&a^{\alpha\beta}=\mathbf{a}^\alpha\cdot\mathbf{a}^\beta,\quad a^{\alpha3}=\mathbf{a}^\alpha\cdot\mathbf{a}^3=0,\quad a^{33}=\mathbf{a}^3\cdot\mathbf{a}^3=1.\end{aligned}\tag{4}$$

$a_{\alpha\beta}$ is also called the coefficient of the first fundamental form of the reference surface. The components of the spatial metric tensor for the shell are related to their counterparts of the reference surface by

$$g_{\alpha\beta}=\mu_\alpha^\omega\mu_\beta^\rho a_{\omega\rho},\quad g_{\alpha3}=g^{\alpha3}=0,\quad g_{33}=g^{33}=1.\tag{5}$$

The displacement vector $\mathbf{V}$ of a material particle can be expressed in terms of the spatial and their shifted components as

$$\mathbf{V}=V_\alpha\mathbf{g}^\alpha+V_3\mathbf{g}^3=v_\alpha\mathbf{a}^\alpha+v_3\mathbf{a}^3,\tag{6}$$

$$V_\alpha=\mu_\alpha^\beta v_\beta,\quad V_3=v_3,\tag{7}$$

and the covariant derivatives of the space components are related with their surface counterparts referred to ${}^{(0)}\Omega$ by [19,20]

$$\begin{aligned}&V_{\alpha\|\beta}=\mu_\alpha^\nu(v_{\nu|\beta}-b_{\nu\beta}v_3),\quad V_{\alpha\|3}=\mu_\alpha^\nu v_{\nu,3},\\&V_{3\|\alpha}=v_{3,\alpha}+b_\alpha^\nu v_\nu,\quad V_{3\|3}=v_{3,3}.\end{aligned}\tag{8}$$

A third-order displacement model for the shell is [16,17]

$$\begin{aligned}v_\alpha(\theta^i;t)&=u_\alpha+\psi_\alpha\theta^3+\varphi_\alpha(\theta^3)^2+\eta_\alpha(\theta^3)^3\\&\quad+\sum_{m=1}^{k-1}\left[{}^{(m)}\Delta v_\alpha+{}^{(m)}u_\alpha(\theta^3-{}^{(m)}h)\right]\mathrm{H}(\theta^3-{}^{(m)}h),\\v_3(\theta^i;t)&=u_3,\end{aligned}\tag{9}$$

where $\mathrm{H}(\theta^3-{}^{(m)}h)$ is the Heaviside step function. The term ${}^{(m)}\Delta v_\alpha$ denotes the jump in the in-surface displacements across the interface ${}^{(m)}\Omega$, is a measure of the damage induced at the interfaces by shear stresses, and vanishes for perfect bonding. Theories for calculating general delamination [21] require additional terms.

Since small initial deviations from the perfect geometry may have a significant influence on the response of structures, we assume that there exists a geometric imperfection in the form of a transverse displacement, V_3^0, in the stress-free reference configuration. The subsequent transverse deflection V_3 is then measured from the imperfect surface. The von Karman partially non-linear components of the Green–St. Venant strain tensor e_{ij},

and the second Piola–Kirchhoff stress components for the shell are [20]:

$$e_{\alpha\beta} = \frac{1}{2}(V_{\alpha\|\beta} + V_{\beta\|\alpha} + V_{3\|\alpha}V_{3\|\beta} + V_{3\|\alpha}V^0_{3\|\beta} + V^0_{3\|\alpha}V_{3\|\beta}),$$
$$e_{\alpha 3} = \frac{1}{2}(V_{\alpha\|3} + V_{3\|\alpha}), \tag{10}$$

$$\sigma^{\alpha\beta} = \mathrm{H}^{\alpha\beta\omega\rho}(e_{\omega\rho} - \alpha_{\omega\rho}T), \quad \sigma^{\alpha 3} = 2E^{\alpha 3\omega 3}e_{\omega 3}, \tag{11}$$

where the temperature increment T in the shell is measured relative to the stress-free reference configuration. $\alpha_{\alpha\beta}$ is the coefficient of linear thermal expansion, E^{ijkl} is the spatial component of the elasticity tensor for an elastic anisotropic body, and $\mathrm{H}^{\alpha\beta\omega\rho} = E^{\alpha\beta\omega\rho} - E^{\alpha\beta 33}E^{33\omega\rho}/E^{3333}$. It is tacitly assumed in Eqs. (10) and (11) that each layer is materially symmetric with respect to surfaces parallel to the reference surface and that σ^{33} is vanishingly small. Batra [22] has shown that for homogeneous simple shear and simple extension of a homogeneous and isotropic elastic body, Eq. (11) predicts physically unreasonable response for large strains. However, for small strains considered here, it is a good representation of the material response.

The boundary conditions on transverse shear stresses on the two bounding surfaces of the shell, and the interface conditions, are now used to reduce the number of unknowns in Eq. (9). In the absence of tangential tractions on ${}^{(0)}\Omega$ and ${}^{(k)}\Omega$, Eqs. (7)–(11) give

$$\psi_\alpha = -u_{3,\alpha} - b^\beta_\alpha u_\beta, \quad \eta_\alpha = d^\beta_\alpha \varphi_\beta + e^\beta_\alpha \sum_{m=1}^{k-1} {}^{(m)}x_\beta, \tag{12}$$

where ${}^{(m)}\mu^\beta_\omega = \mu^\beta_\omega|_{{}^{(m)}\Omega}$, $(\hat{\mu}^{-1})^\beta_\alpha$ is the inverse of $\hat{\mu}^\beta_\alpha = \mu^\beta_\alpha\big|_{\theta^3=2h/3}$, and

$$d^\beta_\alpha = -\frac{2}{3h}\left(\hat{\mu}^{-1}\right)^\omega_\alpha\left(\delta^\beta_\omega - \frac{h}{2}b^\beta_\omega\right), \tag{13a}$$

$$e^\beta_\alpha = -\frac{1}{3h^2}\left(\hat{\mu}^{-1}\right)^\beta_\alpha, \tag{13b}$$

$${}^{(m)}x_\omega = b^\beta_\omega\,{}^{(m)}\Delta v_\beta + {}^{(m)}\mu^\beta_\omega\,{}^{(m)}u_\beta. \tag{13c}$$

The constitutive relation for the elastic interface is a traction-displacement relation. The most general such constitutive relation has the exponential dependence of the normal and shear tractions on the jump in the normal displacement and a sinusoidal dependence of the shear traction on the jump in the tangential displacement [1]. Here, the jump in the normal displacement across an interface is assumed to be zero, and the shear traction at the interface is assumed to depend linearly upon the jump in the tangential displacement. Thus, the interfacial model is good when the jump in the tangential displacement is small as compared with the effective decohesion distance. Thus, at an imperfect interface

$$\sigma^{\beta 3}(\theta^\rho, {}^{(m)}h^+; t) = \sigma^{\beta 3}(\theta^\rho, {}^{(m)}h^-; t), \tag{14a}$$

$${}^{(m)}\mu^\beta_\alpha\,{}^{(m)}\Delta v_\beta = {}^{(m)}R_{\alpha\beta}(\theta^\rho)\sigma^{\beta 3}(\theta^\rho, {}^{(m)}h; t), \quad (m = 1, \ldots, k-1), \tag{14b}$$

where ${}^{(m)}R_{\alpha\beta}$ represents the space compliance coefficient of the mth interface ${}^{(m)}\Omega$. A slight debonding may be modeled by small values of ${}^{(m)}R_{\alpha\beta}$ and ${}^{(m)}R_{\alpha\beta} = 0$ when the mth interface is perfect. As ${}^{(m)}R_{\alpha\beta}$ is a spatial function, non-uniform bonding strength of the interfacial area can be easily characterized. An estimate of the values of interfacial parameters requires a knowledge of the interfacial properties and microstructures. Alternatively, they can be determined either experimentally by direct shear test or through statistically equivalent macroscopic moduli for imperfectly bonded layered media [23]. Improved interface constitutive modeling requires experimental observations and quantitative descriptions of interface deformation and failure mechanisms.

The interface condition (14a) leads to the following $2(k-1)$ linear algebraic equations in the $2(k-1)$ unknowns ${}^{(i)}x_\alpha\,(i = 1, \ldots, k-1)$:

$$\left({}^{(i+1)}E^{\alpha 3\omega 3} - {}^{(i)}E^{\alpha 3\omega 3}\right)\Bigg\{\left[2\delta^\beta_\omega\,{}^{(i)}h - b^\beta_\omega\,{}^{(i)}h^2 + d^\beta_\lambda\left(3\delta^\lambda_\omega\,{}^{(i)}h^2 - 2b^\lambda_\omega\,{}^{(i)}h^3\right)\right]\varphi_\beta + \sum_{m=1}^{i}{}^{(m)}x_\omega + e^\beta_\lambda\left(3\delta^\lambda_\omega\,{}^{(i)}h^2 - 2b^\lambda_\omega\,{}^{(i)}h^3\right)\sum_{m=1}^{k-1}{}^{(m)}x_\beta\Bigg\} + {}^{(i)}E^{\alpha 3\omega 3}\,{}^{(i)}x_\omega = 0, \quad (i = 1, \ldots, k-1), \tag{15}$$

which can be written as

$${}^{(i)}x_\omega = {}^{(i)}f^\lambda_\omega\varphi_\lambda \quad (i = 1, \ldots, k-1). \tag{16}$$

The interface condition (14b) and Eq. (13c) give

$${}^{(i)}\Delta v_\alpha = {}^{(i)}c^\delta_\alpha\varphi_\delta, \quad {}^{(i)}u_\alpha = {}^{(i)}a^\delta_\alpha\varphi_\delta, \quad (i = 1, \ldots, k-1), \tag{17}$$

where

$${}^{(i)}c^\delta_\alpha = \left({}^{(i)}\mu^{-1}\right)^\rho_\alpha\,{}^{(i)}R_{\rho\nu}(\theta^\rho)\,{}^{(i+1)}E^{\nu 3\omega 3}\Bigg\{2\delta^\delta_\omega\,{}^{(i)}h - b^\delta_\omega\,{}^{(i)}h^2 + \sum_{m=1}^{i}{}^{(m)}f^\delta_\omega + \left(3\delta^\lambda_\omega\,{}^{(i)}h^2 - 2b^\lambda_\omega\,{}^{(i)}h^3\right)\times\left(d^\delta_\lambda + e^\beta_\lambda\sum_{m=1}^{k-1}{}^{(m)}f^\delta_\beta\right)\Bigg\},$$
$${}^{(i)}a^\delta_\alpha = \left({}^{(i)}\mu^{-1}\right)^\omega_\alpha\left({}^{(i)}f^\delta_\omega - b^\beta_\omega c^\delta_\beta\right) \quad (i = 1, \ldots, k-1). \tag{18}$$

The coefficients ${}^{(i)}c_\alpha^\delta$ and ${}^{(i)}a_\alpha^\delta$ depend upon the interface properties, the material elasticities and the geometry of laminates.

Substitution of Eqs. (12) and (17) into Eq. (9) leads to

$$v_\alpha(\theta^i;t)=\mu_\alpha^\beta u_\beta-\theta^3 u_{3,\alpha}+h_\alpha^\beta\varphi_\beta,\quad v_3(\theta^i;t)=u_3, \tag{19}$$

where

$$h_\alpha^\beta=\delta_\alpha^\beta(\theta^3)^2+\left(d_\alpha^\beta+e_\alpha^\lambda\sum_{m=1}^{k-1}{}^{(m)}f_\lambda^\beta\right)(\theta^3)^3 +\sum_{m=1}^{k-1}\left[{}^{(m)}c_\alpha^\beta+{}^{(m)}a_\alpha^\beta(\theta^3-{}^{(m)}h)\right]\mathrm{H}(\theta^3-{}^{(m)}h). \tag{20}$$

This ensures the fulfillment of vanishing transverse shear stresses on the two bounding surfaces and the continuity of tractions across interfaces.

It is assumed that the mass density ρ is independent of time t and that arbitrarily distributed normal loads ${}^{(0)}p^3(\theta^\alpha;t)$ and ${}^{(k)}p^3(\theta^\alpha;t)$ are applied to the lower surface ${}^{(0)}\Omega$ and the upper surface ${}^{(k)}\Omega$, respectively. From Hamilton's principle

$$\int_0^{t_0}\left(\int_V\sigma^{ij}\,\delta e_{ij}\,\mathrm{d}V-\int_V\dot{V}^i\,\delta\dot{V}_i\rho\,\mathrm{d}V-\int_\Omega p^3\,\delta V_3\,\mathrm{d}\Omega\right)\mathrm{d}t=0, \tag{21}$$

the following non-linear field equations of motion are derived:

$$\begin{aligned}
&M_{|\beta}^{(1)\alpha\beta}-N^{(1)\alpha}-R^{(1)\alpha}-I^{(1)\beta\alpha}\ddot{u}_\beta+I^{(2)\beta\alpha}\ddot{u}_{3,\beta}-I^{(3)\beta\alpha}\ddot{\varphi}_\beta=0,\\
&M_{|\alpha\beta}^{(2)\alpha\beta}+N^{(1)3}+R_{|\alpha}^{(2)\alpha}+P^3-I^{(1)33}\ddot{u}_3-(I^{(2)\beta\alpha}\ddot{u}_\alpha)_{|\beta}\\
&\quad+(I^{(4)\alpha\beta}\ddot{u}_{3,\alpha})_{|\beta}-(I^{(6)\alpha\beta}\ddot{\varphi}_\alpha)_{|\beta}=0,\\
&M_{|\beta}^{(3)\alpha\beta}-N^{(2)\alpha}-N^{(3)\alpha}-R^{(3)\alpha}-I^{(3)\alpha\beta}\ddot{u}_\beta+I^{(6)\alpha\beta}\ddot{u}_{3,\beta}\\
&\quad-I^{(5)\beta\alpha}\ddot{\varphi}_\beta=0.
\end{aligned} \tag{22}$$

The corresponding boundary conditions are

$$\begin{aligned}
&n_\beta M^{(1)\alpha\beta}=0,\ \text{or}\ \delta u_\alpha=0,\\
&n_\beta\left(M_{|\alpha}^{(2)\beta\alpha}+R^{(2)\beta}-I^{(2)\beta\alpha}\ddot{u}_\alpha+I^{(4)\alpha\beta}\ddot{u}_{3,\alpha}-I^{(6)\alpha\beta}\ddot{\varphi}_\alpha\right)=0,\\
&\quad\text{or}\ \delta u_3=0,\\
&n_\beta M^{(3)\alpha\beta}=0,\ \text{or}\ \delta\varphi_\alpha=0,\\
&n_\beta M^{(2)\alpha\beta}=0,\ \text{or}\ \delta u_{3,\alpha}=0,
\end{aligned} \tag{23}$$

where

$$\left[N^{(1)\alpha},N^{(2)\alpha},N^{(1)3}\right]=\int_0^h\sigma^{\lambda\beta}\mu_\lambda^\nu\left[\mu_{\nu|\beta}^\alpha,h_{\nu|\beta}^\alpha,b_{\nu\beta}\right]\mu\,\mathrm{d}\theta^3,$$

$$N^{(3)\alpha}=\int_0^h\sigma^{\lambda3}\left(\mu_\lambda^\nu h_{\nu,3}^\alpha+b_\lambda^\nu h_\nu^\alpha\right)\mu\,\mathrm{d}\theta^3,$$

$$\left[M^{(1)\alpha\beta},M^{(2)\alpha\beta},M^{(3)\alpha\beta}\right]=\int_0^h\sigma^{\lambda\beta}\mu_\lambda^\nu\left[\mu_\nu^\alpha,\theta^3\,\delta_\nu^\alpha,h_\nu^\alpha\right]\mu\,\mathrm{d}\theta^3,$$

$$\left[R^{(1)\alpha},R^{(2)\alpha},R^{(3)\alpha}\right]=\int_0^h\sigma^{\lambda\beta}\left(V_{3\|\lambda}+V_{3\|\lambda}^0\right)\times\left[b_\beta^\nu\mu_\nu^\alpha,\mu_\beta^\alpha,b_\beta^\nu h_\nu^\alpha\right]\mu\,\mathrm{d}\theta^3, \tag{24}$$

$$\left[I^{(1)\alpha\beta},I^{(2)\alpha\beta},I^{(3)\alpha\beta},I^{(4)\alpha\beta},I^{(5)\alpha\beta},I^{(6)\alpha\beta}\right]=\int_0^h\rho a^{\lambda\nu}\left[\mu_\nu^\alpha\mu_\lambda^\beta,\theta^3\,\delta_\nu^\alpha\mu_\lambda^\beta,h_\nu^\alpha\mu_\lambda^\beta,(\theta^3)^2\,\delta_\nu^\alpha\delta_\lambda^\beta,h_\nu^\alpha h_\lambda^\beta,\theta^3h_\nu^\alpha\delta_\lambda^\beta\right]\mu\,\mathrm{d}\theta^3,$$

$$I^{(1)33}=\int_0^h\rho\mu\,\mathrm{d}\theta^3, \tag{25}$$

$$P^3={}^{(k)}\mu^{(k)}p^3+{}^{(0)}p^3. \tag{26}$$

For brevity, the governing equations written in terms of displacements are omitted. The non-linear static field equations [16] and linear dynamic field equations [17] for the shell under mechanical loads can be retrieved as special cases of Eq. (22).

3. Illustrative examples and discussions

Because of the complexity of the governing equations, only a linear static case is considered. Since the response of a shell under mechanical loads has been reported in [16,17], the numerical examples studied herein are restricted to considering only thermal effects. A circular cylindrical laminated shell with inner radius r_0, length L and central angle Φ, is considered in the example problems. The cylindrical panel is simply supported at edges $\theta^1=0$, L and $\theta^2=0$, Φ. Uniform interfacial imperfections are assumed. The laminated shell consists of three layers of equal thickness. Each layer has unidirectionally aligned fibers with the following elastic moduli [24]:

$$\begin{aligned}
&E_L=172.5\ \text{GPa},\quad E_T=6.9\ \text{GPa},\\
&G_{LT}=3.45\ \text{GPa},\quad G_{TT}=1.38\ \text{GPa},\\
&\nu_{LT}=\nu_{TT}=0.25,
\end{aligned} \tag{27}$$

where E is the tensile modulus, G the shear modulus, ν Poisson's ratio and the subscripts L and T refer, respectively, to the directions parallel and normal to the fibers.

The temperature field is assumed to be given by

$$T=\hat{T}(\theta^3)\sin\frac{m_1\pi\theta^1}{L}\sin\frac{m_2\pi\theta^2}{\Phi}. \tag{28}$$

A closed-form solution of the linear thermally-induced bending problem is of the form

$$[u_1, \varphi_1] = [U_1, \Phi_1] \cos\frac{m_1\pi\theta^1}{L} \sin\frac{m_2\pi\theta^2}{\Phi},$$
$$[u_2, \varphi_2] = [U_2, \Phi_2] \sin\frac{m_1\pi\theta^1}{L} \cos\frac{m_2\pi\theta^2}{\Phi}, \tag{29}$$
$$u_3 = U_3 \sin\frac{m_1\pi\theta^1}{L} \sin\frac{m_2\pi\theta^2}{\Phi}.$$

For brevity, the procedure for obtaining the closed form solution is omitted. The physical components of tensors are related to their tensorial counterparts as

$$^{(m)}R_{\langle\alpha\beta\rangle} = \frac{1}{\sqrt{g_{AA}g_{BB}}}\,^{(m)}R_{\alpha\beta},$$
$$V_{\langle i\rangle} = v_{\langle i\rangle} = \frac{1}{\sqrt{a_{II}}}v_i, \tag{30}$$
$$e_{\langle ij\rangle} = \frac{1}{\sqrt{g_{II}g_{JJ}}}e_{ij}, \quad \sigma_{\langle ij\rangle} = \sqrt{g_{II}g_{JJ}}\sigma^{ij},$$

where an upper case subscript takes the same value as the corresponding lower case index, and no implicit summation applies to repeated indices. The physical quantities are then non-dimensionalized by

$$S = \frac{r_0}{h} + 0.5, \quad \bar{T} = \frac{T}{\hat{T}^+}, \quad \bar{V}_{\langle i\rangle} = \frac{V_{\langle i\rangle}}{h\alpha^*\hat{T}^+},$$
$$\bar{\sigma}_{\langle ij\rangle} = \frac{\sigma_{\langle ij\rangle}}{E_T\alpha^*\hat{T}^+}, \tag{31}$$

where $\hat{T}^+$ is the amplitude of the temperature on the upper surface of the shell.

In the first example, computed results for a perfectly bonded (0°/90°/0°) circular cylindrical shell under a constant through-thickness distribution of $\hat{T}$ are presented in Table 1. The following parameters are used for the calculation:

$$L/h = 10S, \quad \Phi = 2\pi, \quad m_1 = 1, \quad m_2 = 2,$$
$$\alpha_T/\alpha_L = 3, \quad \alpha^* = \alpha_L. \tag{32}$$

These results are compared with those given in [25] using the classical shell theory (CST), the first-order shear deformation theory (FSDT) and the higher-order shear deformation theory (HSDT) [26], where an approximation of the Lamé parameters was taken. For perfect interfaces, the present results correspond to those obtained by using the third-order zigzag theory for a perfectly bonded circular cylindrical shell [27,28]. However, only results for mechanical loads obtained by using the zigzag theory were given. It is seen that for small values of S, the zigzag theory predicts results noticeably different from those obtained with the CST, FSDT and HSDT. In particular, the errors in the stresses are quite large. As the continuity conditions of both displacements and tractions at the interfaces are satisfied in the zigzag model, it should predict better results than those obtained with the other three theories. Moreover, because the approximation of the Lamé parameters was taken in [25,26], the corresponding results are only appropriate for a shallow shell. For a thin shallow shell, e.g. $S = 100$, all of these theories give essentially the same results.

In the second example we present results for an infinitely long laminated panel (90°/0°/90°), for which the following parameters are used [29]:

$$\alpha_L = 0.57 \times 10^{-6}/\mathrm{K}, \quad \alpha_T = 35.6 \times 10^{-6}/\mathrm{K},$$
$$\kappa_L = 36.42\ \mathrm{W/mK}, \quad \kappa_T = 0.96\ \mathrm{W/mK},$$
$$L \to \infty, \quad \Phi = \frac{\pi}{3}, \quad m_2 = 1, \tag{33}$$
$$^{(m)}R_{\langle\alpha\beta\rangle} = \delta_{\alpha\beta}\frac{\bar{R}h}{E_T}, \quad ^{(m)}R^T = \frac{\bar{R}^T h}{\kappa^*},$$
$$\alpha^* = 10^{-6}/K, \quad \kappa^* = 1\ \mathrm{W/mK}.$$

Here κ denotes the thermal conductivity of the composite. Equal degree of mechanical interfacial imperfection is assumed at each interface, with $\bar{R}$ being a dimensionless quantity. Similarly, identical thermal interfacial imperfection is characterized by the dimensionless quantity $\bar{R}^T$. The temperature field within the panel is obtained by solving the heat conduction equation and the details are given in the Appendix A.

Figs. 2–5 depict the through-thickness distributions of the dimensionless temperature $\bar{T}$, displacement $\bar{V}_{\langle 2\rangle}$, longitudinal stress $\bar{\sigma}_{\langle 22\rangle}$ and transverse shear stress $\bar{\sigma}_{\langle 23\rangle}$ in the panel ($S = 6$) for different degrees of interfacial imperfections. Note that these quantities are independent of θ^1 because the cylindrical panel is infinitely long. Unlike the case of mechanical loads [16,17], the mechanical imperfection characterized by different values

Table 1
Comparison of results obtained by using different theories for a three-ply (0°/90°/0°) laminated circular cylindrical shell with perfect interfaces ($L/h = 10S, \Phi = 2\pi, m_1 = 1, m_2 = 2$)[a]

S		CST	FSDT	HSDT	Present (zigzag)
10	$\bar{V}_{\langle 3\rangle}(L/2, \pi/2, h)/S^2$	1.1280	1.1284	1.1284	1.1792
	$\bar{\sigma}_{\langle 11\rangle}(L/2, \pi/2, h)/S$	0.2157	0.2147	0.2147	0.2332
	$\bar{\sigma}_{\langle 22\rangle}(L/2, \pi/2, h)/S$	−0.1251	−0.1255	−0.1254	−0.1812
100	$\bar{V}_{\langle 3\rangle}(L/2, \pi/2, h)/S^2$	0.1186	0.1186	0.1186	0.1187
	$\bar{\sigma}_{\langle 11\rangle}(L/2, \pi/2, h)/S$	0.0111	0.0111	0.0111	0.0110
	$\bar{\sigma}_{\langle 22\rangle}(L/2, \pi/2, h)/S$	−0.0176	−0.0176	−0.0176	−0.0182

[a] CST, FSDT and HSDT results are given by Khdeir [25].

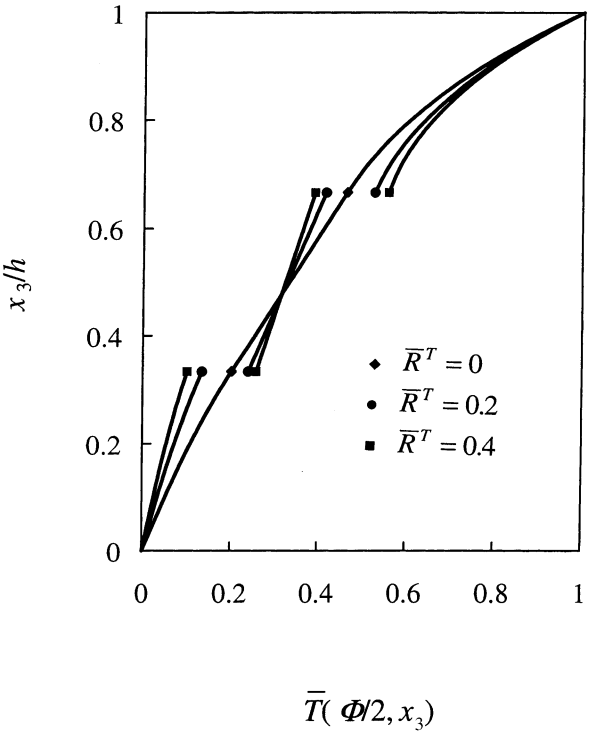

Fig. 2. Through-the-thickness variation of the temperature field in an infinitely long three-ply (90°/0°/90°) laminated circular cylindrical panel ($L \to \infty, S = 6, \Phi = \pi/3, m_2 = 1$).

of $\bar{R}$ has only slight effect on the response of the panel to the thermal load. However, the thermal contact resistance characterized by different values of $\bar{R}^T$ has a noticeable effect on the in-surface displacement, the longitudinal stress and the transverse shear stress in the panel. Tables 2 and 3 give the central deflection of the cylindrical and the corresponding flat panel for progressively higher values of the interfacial imperfection. The thermal contact resistance $\bar{R}^T$ has a significant effect on the deflection for various values of $\bar{R}$ and S. The stiffness degradation of the panel for the problem considered, i.e., an increase in the value of $\bar{R}$ only changes the deflection for a relatively thick panel, $S = 4$.

4. Conclusions

Non-linear equations of motion governing the thermoelastic response of a laminated shell containing interfacial imperfections have been derived by using the Hamilton principle. The vanishing of transverse shear stresses at the two bounding surfaces of the shell and the continuity of tangential tractions at the interfaces between adjoining layers have been used to reduce the number of unknowns in the assumed third-order displacement model. Numerical results computed for a linear static problem indicate that the thermal interfacial imperfections have a noticeable effect on the thermo-

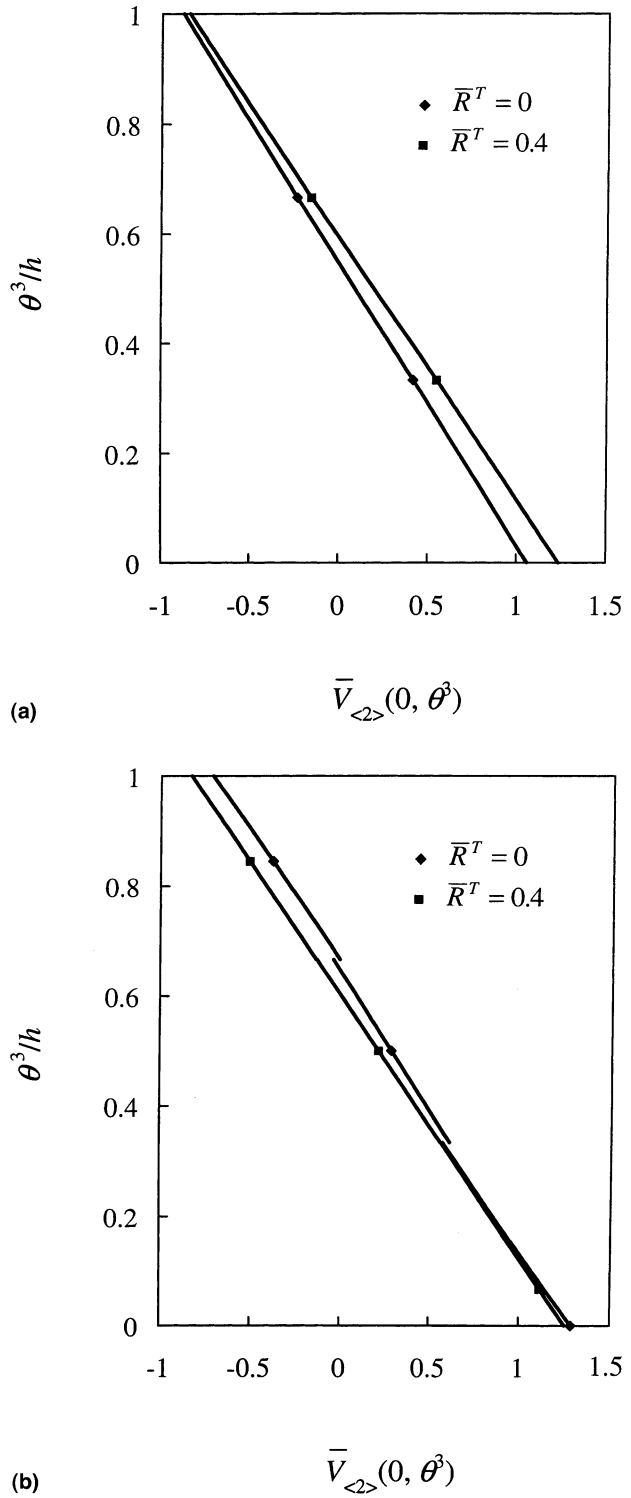

Fig. 3. Through-the-thickness variation of the in-surface displacement of an infinitely long three-ply (90°/0°/90°) laminated circular cylindrical panel with: (a) $\bar{R} = 0$; and (b) $\bar{R} = 0.9$ ($L \to \infty, S = 6, \Phi = \pi/3, m_2 = 1$).

mechanical response of the panel. However, the deformations of the panel are not very sensitive to the mechanical imperfections at the interfaces.

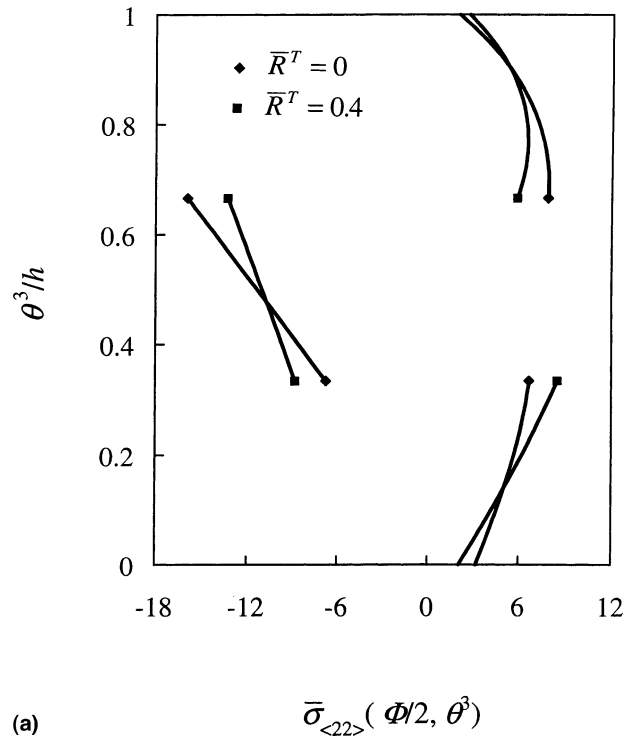

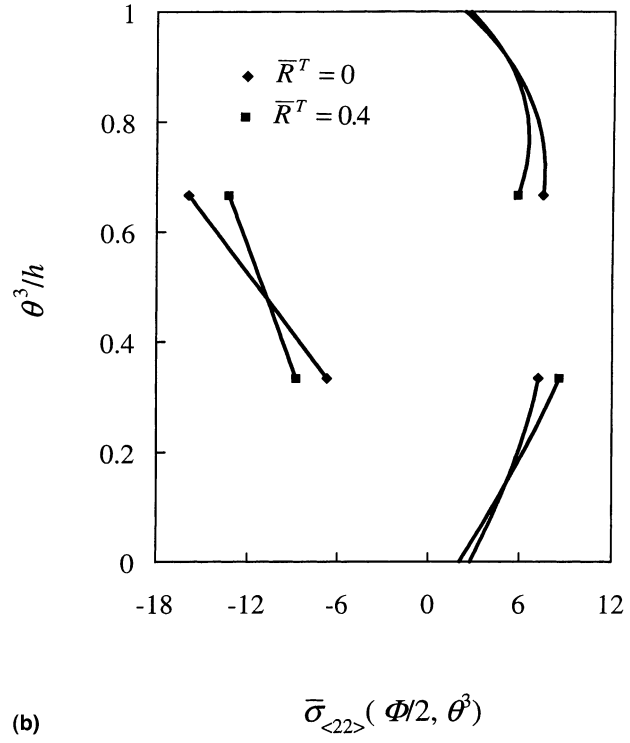

Fig. 4. Through-the-thickness variation of the bending stress in an infinitely long three-ply (90°/0°/90°) laminated circular cylindrical panel with: (a) $\bar{R} = 0$; and (b) $\bar{R} = 0.9$ $(L \to \infty, S = 6, \Phi = \pi/3, m_2 = 1)$.

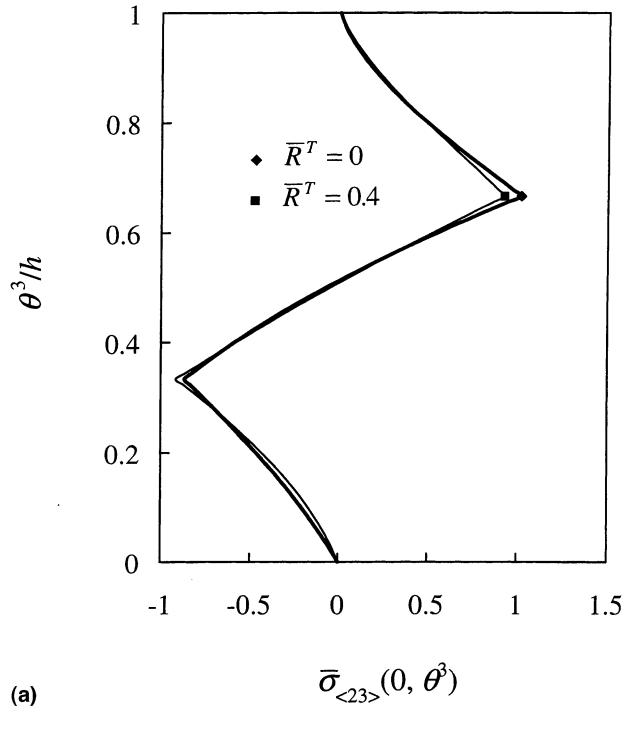

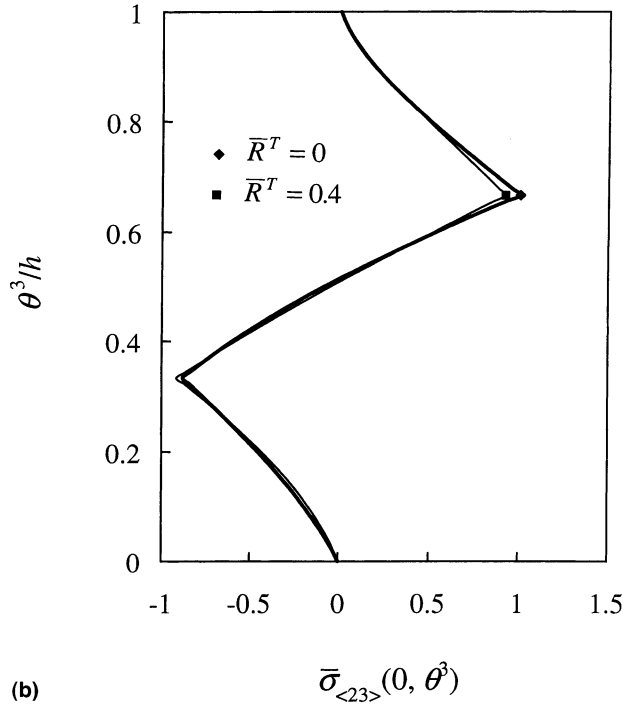

Fig. 5. Through-the-thickness variation of the transverse shear stress in an infinitely long three-ply (90°/0°/90°) laminated circular cylindrical panel with: (a) $\bar{R} = 0$; and (b) $\bar{R} = 0.9$ $(L \to \infty, S = 6, \Phi = \pi/3, m_2 = 1)$.

Appendix A. Solution for the heat conduction problem

An infinitely long cross-ply laminated circular cylindrical panel with inner radius r_0 and central angle Φ is subjected to the following thermal loads on the top and bottom surfaces and the thermal boundary conditions:

$$T(\theta^2, r_0) = \hat{T}^- \sin\frac{m_2\pi\theta^2}{\Phi}, \tag{A.1a}$$

Table 2
Effect of interfacial imperfections on the central deflection of a three-ply (90°/0°/90°) infinitely long laminated circular cylindrical panel ($L \to \infty, \Phi = \pi/3, m_2 = 1$)

S	$\bar{R}^T$	$\bar{R} = 0$	$\bar{R} = 0.3$	$\bar{R} = 0.6$	$\bar{R} = 0.9$
4	0	1.6137	1.7598	1.9123	2.0543
	0.2	1.6601	1.7476	1.8367	1.9189
	0.4	1.6828	1.7403	1.7985	1.8514
10	0	11.530	11.674	11.883	12.146
	0.2	12.308	12.318	12.352	12.407
	0.4	12.733	12.669	12.608	12.550
50	0	305.13	305.23	305.40	305.64
	0.2	330.88	330.81	330.75	330.71
	0.4	345.42	345.26	345.08	344.88

Table 3
Effect of interfacial imperfections on the central deflection of a three-ply (90°/0°/90°) infinitely long laminated flat panel with width b ($L \to \infty, m_2 = 1$)

b/h	$\bar{R}^T$	$\bar{R} = 0$	$\bar{R} = 0.3$	$\bar{R} = 0.6$	$\bar{R} = 0.9$
4	0	1.2197	1.3494	1.4849	1.6105
	0.2	1.2538	1.3397	1.4286	1.5107
	0.4	1.2703	1.3350	1.4015	1.4626
10	0	9.1724	9.2722	9.4268	9.6267
	0.2	9.7808	9.7645	9.7693	9.7929
	0.4	10.113	10.033	9.9560	9.8835
50	0	247.24	247.31	247.45	247.65
	0.2	268.08	268.01	267.95	267.90
	0.4	279.85	279.70	279.53	279.34

$$T(\theta^2, r_0 + h) = \hat{T}^{+} \sin\frac{m_2\pi\theta^2}{\Phi}, \tag{A.1b}$$

$$T(0, \theta^3) = 0, \tag{A.1c}$$

$$T(\Phi, \theta^3) = 0, \tag{A.1d}$$

where $\hat{T}^{\pm}$ denote the amplitudes of the prescribed temperature on the top and bottom surfaces of the panel. The temperature field at any point of the panel is given by

$$T(\theta^2, \theta^3) = {}^{(1)}T\,\mathrm{H}(\theta^3) + \sum_{m=1}^{k-1} \left({}^{(m+1)}T - {}^{(m)}T\right)\mathrm{H}(\theta^3 - {}^{(m)}h). \tag{A.2}$$

The temperature ${}^{(m)}T$ in the mth ply ($m = 1, \ldots, k$) satisfies the steady-state heat conduction equation

$${}^{(m)}\kappa_{\langle 22\rangle}\frac{1}{(r_0+\theta^3)^2}{}^{(m)}T_{,22} + {}^{(m)}\kappa_{\langle 33\rangle}\left({}^{(m)}T_{,33} + \frac{1}{r_0+\theta^3}{}^{(m)}T_{,3}\right) = 0, \tag{A.3}$$

where ${}^{(m)}\kappa_{\langle 22\rangle}$ and ${}^{(m)}\kappa_{\langle 33\rangle}$ are, respectively, the physical components in the θ^2- and θ^3-directions of the thermal conductivity tensor for the mth ply. Subject to the boundary conditions (A.1a)–(A.1d), the temperature in the mth ply can be taken to be

$${}^{(m)}T(\theta^2, \theta^3) = {}^{(m)}\hat{T}(\theta^3)\sin\frac{m_2\pi\theta^2}{\Phi}, \tag{A.4}$$

where

$${}^{(m)}\hat{T} = \left\{ {}^{(m)}\hat{T}^{+}\left[\left(\frac{r_0+\theta^3}{r_0+{}^{(m-1)}h}\right)^{{}^{(m)}\lambda} - \left(\frac{r_0+{}^{(m-1)}h}{r_0+\theta^3}\right)^{{}^{(m)}\lambda}\right] - {}^{(m)}\hat{T}^{-}\left[\left(\frac{r_0+\theta^3}{r_0+{}^{(m)}h}\right)^{{}^{(m)}\lambda} - \left(\frac{r_0+{}^{(m)}h}{r_0+\theta^3}\right)^{{}^{(m)}\lambda}\right]\right\} \Bigg/ \left[\left(\frac{r_0+{}^{(m)}h}{r_0+{}^{(m-1)}h}\right)^{{}^{(m)}\lambda} - \left(\frac{r_0+{}^{(m-1)}h}{r_0+{}^{(m)}h}\right)^{{}^{(m)}\lambda}\right],$$

$${}^{(m)}\lambda = \sqrt{\frac{{}^{(m)}\kappa_{\langle 22\rangle}}{{}^{(m)}\kappa_{\langle 33\rangle}}}\frac{m_2\pi}{\Phi}, \tag{A.5}$$

and ${}^{(m)}\hat{T}^{\pm}$ equals the value of ${}^{(m)}\hat{T}$ on the top and bottom surfaces of the mth ply. The temperature field (A.4) identically satisfies Eq. (A.3).

By assuming the condition of imperfect thermal contact between adjacent plies [30], i.e.,

$$
\begin{aligned}
&{}^{(m+1)}T^{-} - {}^{(m)}T^{+} = {}^{(m)}R^{T}\,{}^{(m+1)}\kappa_{\langle 33\rangle}\,{}^{(m+1)}T_{,3},\\
&{}^{(m+1)}\kappa_{\langle 33\rangle}\,{}^{(m+1)}T^{-}_{,3} = {}^{(m)}\kappa_{\langle 33\rangle}\,{}^{(m)}T^{+}_{,3},\ \text{at } \theta^{3} = {}^{(m)}h\\
&(m = 1,\ldots,k-1),
\end{aligned}
\tag{A.6}
$$

we have

$$
\begin{aligned}
&\frac{1}{{}^{(m)}R^{T}}\left({}^{(m+1)}\hat{T}^{-} - {}^{(m)}\hat{T}^{+}\right)\\
&\quad = \frac{1}{r_0 + {}^{(m)}h}\left({}^{(m+1)}B^{(m+1)}\hat{T}^{+} + {}^{(m+1)}A^{(m+1)}\hat{T}^{-}\right)\\
&\quad = -\frac{1}{r_0 + {}^{(m)}h}\left({}^{(m)}A^{(m)}\hat{T}^{+} + {}^{(m)}B^{(m)}\hat{T}^{-}\right),
\end{aligned}
\tag{A.7}
$$

where

$$
\begin{aligned}
{}^{(m)}A = &-{}^{(m)}\lambda^{(m)}\kappa_{\langle 33\rangle}\left[\left(\frac{r_0 + {}^{(m)}h}{r_0 + {}^{(m-1)}h}\right)^{{}^{(m)}\lambda}\right.\\
&\left.+\left(\frac{r_0 + {}^{(m-1)}h}{r_0 + {}^{(m)}h}\right)^{{}^{(m)}\lambda}\right]\Bigg/\left[\left(\frac{r_0 + {}^{(m)}h}{r_0 + {}^{(m-1)}h}\right)^{{}^{(m)}\lambda}\right.\\
&\left.-\left(\frac{r_0 + {}^{(m-1)}h}{r_0 + {}^{(m)}h}\right)^{{}^{(m)}\lambda}\right],
\end{aligned}
$$

$$
\begin{aligned}
{}^{(m)}B = 2\,{}^{(m)}\lambda^{(m)}\kappa_{\langle 33\rangle}&\left\{1\Bigg/\left[\left(\frac{r_0 + {}^{(m)}h}{r_0 + {}^{(m-1)}h}\right)^{{}^{(m)}\lambda}\right.\right.\\
&\left.\left.-\left(\frac{r_0 + {}^{(m-1)}h}{r_0 + {}^{(m)}h}\right)^{{}^{(m)}\lambda}\right]\right\}.
\end{aligned}
\tag{A.8}
$$

The interlayer thermal contact resistance ${}^{(m)}R^{T}$ is defined as the reciprocal of the interlayer thermal conductance. For perfect interlayer contact, ${}^{(m)}R^{T} = 0$. A non-zero value of ${}^{(m)}R^{T}$ corresponds to the mth interface being thermally imperfect. The $2k$ unknowns ${}^{(m)}\hat{T}^{\pm}$ $(m = 1,\ldots,k)$ can be determined from the $2k$ linear equations Eqs. (A.7), (A.1a) and (A.1b).

References

[1] Needleman A. Micromechanical modeling of interfacial decohesion. Ultramicroscopy 1992;40:203–14.

[2] Aboudi J. Damage in composites – Modelling of imperfect bonding. Compos Sci Tech 1987;28:103–28.

[3] Cheng ZQ, Jemah AK, Williams FW. Theory for multilayered anisotropic plates with weakened interfaces. J Appl Mech 1996;63:1019–26.

[4] Cheng ZQ, Kennedy D, Williams FW. Effect of interfacial imperfection on buckling and bending behavior of composite laminates. AIAA J 1996;34:2590–5.

[5] Cheng ZQ, Howson WP, Williams FW. Modelling of weakly bonded laminated composite plates at large deflections. Int J Solids Struct 1997;34:3583–99.

[6] Cheng ZQ, Kitipornchai S. Prestressed composite laminates featuring interlaminar imperfection. Int J Mech Sci 2000;42:425–43.

[7] Schmidt R, Librescu L. Geometrically nonlinear theory of laminated anisotropic composite plates featuring interlayer slips. Nova J Math Game Theory Algebra 1996;5:131–47.

[8] Di Sciuva M. Geometrically nonlinear theory of multilayered plates with interlayer slips. AIAA J 1997;35:1753–9.

[9] Bai QS, Murakami S, Kanagawa Y. A lamination theory incorporating the effect of interlaminar deformation. J Compos Mater 1997;31:2052–73.

[10] Williams TO, Addessio FL. A general theory for laminated plates with delaminations. Int J Solids Struct 1997;34:2003–24.

[11] Williams TO, Addessio FL. A dynamic model for laminated plates with delaminations. Int J Solids Struct 1998;35:83–106.

[12] Williams TO. A generalized multilength scale nonlinear composite plate theory with delamination. Int J Solids Struct 1999;36:3015–50.

[13] Di Sciuva M, Icardi U, Librescu L. Effects of interfacial damage on the global and local static response of cross-ply laminates. Int J Fracture 1999;96:17–35.

[14] Icardi U. Free vibration of composite beams featuring interlaminar bonding imperfections and exposed to thermomechanical loading. Compos Struct 1999;46:229–43.

[15] Icardi U, Di Sciuva M, Librescu L. Dynamic response of adaptive cross-ply cantilevers featuring interlaminar bonding imperfections. AIAA J 2000;38:499–506.

[16] Cheng ZQ, Kitipornchai S. Nonlinear theory for composite laminated shells with interfacial damage. J Appl Mech 1998;65:711–8.

[17] Cheng ZQ, He LH, Kitipornchai S. Influence of imperfect interfaces on bending and vibration of laminated composite shells. Int J Solids Struct 2000;37:2127–50.

[18] Schmidt R, Librescu L. A general theory of geometrically imperfect laminated composite shells featuring damaged bonding interfaces. Q J Mech Appl Math 1999;52:565–83.

[19] Naghdi PM. Foundation of elastic shell theory. In: Sneddon IN, Hill R, editors. Progress of solid mechanics, vol. 4. Amsterdam: North-Holland; 1963.

[20] Librescu L. Elastostatics and kinetics of anisotropic and heterogeneous shell-type structures. Leyden, Netherlands: Noordhoff; 1975.

[21] Gu HZ, Chattopadhyay A. Delamination buckling and post-buckling of composite cylindrical shells. AIAA J 1996;34:1279–86.

[22] Batra RC. Linear constitutive relations in isotropic finite elasticity. J Elasticity 1998;51:243–5.

[23] Lai YS, Wang CY, Tien YM. Micromechanical analysis of imperfectly bonded layered media. J Eng Mech 1997;123:986–95.

[24] Pagano NJ. Exact solutions for composite laminates in cylindrical bending. J Compos Mater 1969;3:398–411.

[25] Khdeir AA. Thermoelastic analysis of cross-ply laminated circular cylindrical shells. Int J Solids Struct 1996;33:4007–17.

[26] Reddy JN, Liu CF. A higher-order shear deformation theory of laminated elastic shells. Int J Eng Sci 1985;23:319–30.

[27] He LH. A linear theory of laminated shells accounting for continuity of displacements and transverse shear stresses at layer interfaces. Int J Solids Struct 1994;31:613–27.

[28] Di Sciuva M, Icardi U. Discrete-layer models for multilayered shells accounting for interlayer continuity. Meccanica 1993;28:281–91.

[29] Tungikar VB, Rao KM. Three-dimensional exact solution of thermal stresses in rectangular composite laminate. Compos Struct 1994;27:419–30.

[30] Chen TC, Jang HI. Thermal stresses in a multilayered anisotropic medium with interface thermal resistance. J Appl Mech 1995;62:810–1.